Lamellar Structures of Symmetric Diblock Copolymers: Comparisons between Lattice Monte Carlo Simulations and Self-Consistent Mean-Field Calculations

Qiang Wang, Paul F. Nealey, and Juan J. de Pablo*

Department of Chemical Engineering, University of Wisconsin−Madison, Madison, Wisconsin 53706-1691

Received March 14, 2002; Revised Manuscript Received August 30, 2002

ABSTRACT: We have conducted detailed comparisons of the predictions of self-consistent mean-field (SCMF) theory with results of Monte Carlo simulations for bulk lamellar structures of symmetric diblock copolymers A−B in concentrated solutions. Large differences are found among the values of the Flory−Huggins parameter extracted in different ways. Under the convolution approximation, we assess the accuracy of the SCMF theory by comparing simulated lamellar profiles with those obtained from the theory. A Flory−Huggins parameter inferred from the free energy of the system provides good overall agreement between simulated and theoretical lamellar profiles. The results of simulations for chain dimensions scale with the product ϵN, where ϵ denotes the repulsion between A and B segments, and N is the chain length.

1. Introduction

Diblock copolymer molecules consist of two distinct polymer chains (blocks) covalently bonded at one end. Because of the connectivity constraints and the incompatibility between the two blocks, diblock copolymers spontaneously self-assemble into microphase-separated domains that exhibit ordered morphologies at temperatures below the order−disorder transition (ODT).[1] In the case of symmetric diblock copolymers where the two blocks have the same volume fraction, the ordered structure consists of lamellae of spatially alternating A-rich and B-rich layers. Such lamellae have been studied extensively, both by molecular simulations and theory, largely as a result of their simple one-dimensional structure and the inherent symmetry. Following the seminal work of Helfand,[2] Helfand and Wasserman,[3−5] and Leibler[6] on the microphase separation of block copolymers, several theories have been proposed to study these materials; of these, the self-consistent mean-field (SCMF) theory is perceived by many as providing one of the more satisfactory descriptions of copolymer systems, including melts, solutions, blends, and, very recently, copolymer/nanoparticle systems.[7−9] Readers are referred to refs 10 and 11 for reviews of the SCMF theory. As is the case for any theoretical formalism, however, the SCMF theory is built on a number of assumptions that must be closely scrutinized in order to determine its predictive ability, and to further improve its accuracy. For example, the SCMF theory employs a Gaussian thread model of polymer chains to describe the entropy of the system, and it adopts a Flory−Huggins interaction parameter χ_{AB} to account for energetic contributions to the free energy of the system. The theory does not take into account fluctuation effects, and generally ignores equation-of-state (compressibility) effects. In the case of solutions, chain-swelling effects are also neglected. Much of our work is concerned with applications of block copolymers to nanopatterning, where low molecular weight polymers must be used to achieve the target length scales of tens of nanometers. In these cases, it is unclear if and to what extent the SCMF theory can provide accurate predictions. In view of the qualitative success of the SCMF theory in describing experimental data for high molecular weights, it is of interest to explore the consequences of some of its approximations, and to examine its accuracy for low to intermediate molecular weights. Molecular simulations (Monte Carlo simulations and molecular dynamics) are attractive in this regard because they can provide "exact" solutions for model systems. Furthermore, some quantities that are difficult to determine in experiments or in theory are readily accessible in simulations. Several groups have reported results of simulations for symmetric diblock copolymers in the bulk (either in melts or in concentrated solutions);[12−32] bulk simulations on cylinder-forming[28,33−36] and sphere-forming[35] asymmetric diblock copolymers have also been reported. Most of these are lattice Monte Carlo simulations performed at constant number of copolymer chains; exceptions to this trend are provided by our previous work,[32,36] in which lattice Monte Carlo simulations were performed in an expanded grand-canonical ensemble, and by the work of Kremer et al.,[27,30] in which molecular dynamics were performed at constant pressure. For the more widely studied case of symmetric diblock copolymers in concentrated solutions or melts (characterized by a copolymer segmental density $\bar{\phi}_C \geq 0.5$), we briefly summarize those lattice Monte Carlo simulations in Table 1.

A significant contribution of molecular simulations has been to examine one of the key underlying assumptions in Leibler's theory, namely that copolymer chain conformations remain Gaussian despite the energetic repulsion between A and B segments[6]. Deviations from the Gaussian conformation, even at temperatures well above the ODT, were originally identified in simulations by Binder and co-workers,[13−15,33] and subsequently in other simulation studies.[16−18,21,23,25−31,35,36] Fried and

* To whom correspondence should be addressed

10.1021/ma0203905 CCC: $22.00
Published on Web 11/08/2002

Table 1. List of Published Lattice Monte Carlo Simulations on Thermodynamic Behavior of Symmetric Diblock Copolymers in Concentrated Solutions or Melts[i]

ref	lattice[a]	box size	N	$\bar{\phi}_C$	interactions[b]
12	SQL	128^2	10−40	0.6	$\epsilon_{AA} = \epsilon_{BB} = -2k_BT$
20	2*d*BFM1×	44^2	$A_{10}B_{11}$	0.9545	ϵ_{AB}
14,15	SCL	$(16-32)^3$	16−60	0.8	$\epsilon_{AB} \geq 0$
16[c]	FCC	20^3	20−50	0.6−1	$\epsilon_{AB} \geq 0$
17[d]	SCL	22^3	20	0.845	$\epsilon_{AB} \geq 0$
18, 23	SCL	$(17-30)^3$	36, 60	0−0.76	$\epsilon_{AA} < 0$, $\epsilon_{BB} < 0$
21, 22	BFM1×	$(17-112)^3$	6−192	0.6−0.9	$\epsilon_{AB} \geq 0$
24	SCL	22^3	20	0.45−0.85	$\epsilon_{AB} = \epsilon_{AV} > 0$
25[f]	BFM1	$(27-45)^3$	20−80	0.5	$\epsilon_{AB} = (4-4.48)k_BT$
26	BFM1×	40^3	16	0.8	$\epsilon_{AB} \geq 0$
28	FCC	$30 \times 30 \times 40$	20, 40	1	$\epsilon_{AB} > 0$
29[g]	BFM	$50 \times 50 \times L_z$	16−48	0.6	$\epsilon_{AB} \geq 0$
31	BFM1×	50^3	20	0.6	$\epsilon_{AB} \geq 0$
32[h]	SCL	$L_x \times L_y \times L_z$	24	0.8	$\epsilon_{AB} = (0.417-0.455)k_BT$

[a] Abbreviations for different lattice models: two-dimensional square lattice (SQL); two-dimensional single-site bond fluctuation model with bond-crossing (2*d* BFM1×); simple cubic lattice (SCL); face-centered cubic lattice (fcc); bond fluctuation model (BFM); single-site bond fluctuation model without bond-crossing (BFM1) and with bond-crossing (BFM1×). [b] Vacancies are denoted by V; all other interactions are set to zero; refer to section 2.1.1 or original papers for details. [c] Chain length $N = 100$ was used in some cases. [d] Boxes of $(24-44)^3$ were used in some cases at $\epsilon_{AB} = 0.5k_BT$. [e] Vacancies were treated as A and B monomers of equal amount. [f] All simulations were below the ODT. [g] 1600 chains were confined between two repulsive walls separated by $L_z = 135-410$ (adjusted according to chain length N). [h] Rectangular boxes with $L_x \neq L_y \neq L_z$ were used; all simulations were below the ODT. [i] Please refer to the original papers for details.

Binder also proposed approximate scaling relations for static properties of copolymers (which will be discussed in detail in section 3.7), and identified a collective length scale for compositional fluctuations.[14,15,33] In two-dimensional simulations, Yang and co-workers demonstrated that A and B segments mix in a nonrandom manner due to the chain connectivity, thereby implying a difference in the values of χ_{AB} for the diblock copolymer and the corresponding homopolymer blend.[20] Using a single-site bond fluctuation model,[37], Larson reported a qualitative change in the order−disorder transition and compositional fluctuations at chain length $N \approx 50$.[21,22] More recently, Pakula identified in simulations a temperature (above the ODT) at which diblock copolymers exhibit a crossover from a homogeneous state to a state with considerably larger compositional fluctuations.[28] The dynamic behavior of diblock copolymers has also been studied by molecular simulations.[19,24,25,28−30,35] As noted above, most simulations of ordered block copolymer structures have been conducted at constant volume. In view of the large finite-size effects encountered in these systems, constant-volume studies can only provide qualitative or semiquantitative results regarding the ODT temperature and the equilibrium bulk period L_0.[32,36,38] To our knowledge, the only published constant-pressure simulations of diblock copolymers were performed by Kremer and co-workers, who studied dense melts of symmetric diblock copolymers by molecular dynamics.[27,30] They confirmed the scaling of $L_0 \propto N^{2/3}$ in the strong segregation regime, but the problem of accurately determining the ODT from simulations remains unsolved.[27,30,38]

Ironically, most comparisons between simulations and theory have been restricted to the ODT temperature;[13,14,16,18,21,22,31] these studies have focused on weak segregation theories, i.e., theories by Leibler,[6] by Fredrickson and Helfand,[39] and by Barrat and Fredrickson.[40] To the best of our knowledge, the only quantitative comparisons between the SCMF theory and simulations were reported by Geisinger et al., who studied thin films of symmetric diblock copolymers confined between two homogeneous and identical surfaces.[41,42] Their study assumed that χ_{AB} is proportional to the parameter used to quantify the repulsion between A and B segments in simulations.[41,42]

The work presented here differs from earlier studies in several important respects. First, we consider bulk systems, as opposed to confined films. Second, our simulations are performed at constant chemical potential, thereby allowing us to compare the SCMF theory and simulations on the basis of the free energy of the system. Third, our theoretical calculations take the solvent into account, which provides an additional test of the predictive capability of the theory. In contrast to ODT-based comparisons, our simulations are performed at temperatures below the ODT. The problem of accurately determining L_0 is also avoided by making comparisons for lamellae at some *specified* period L, instead of L_0.

2. Models

2.1. Lattice Monte Carlo Simulations. Our Monte Carlo simulations are performed in an expanded grand-canonical ensemble in the framework of a simple cubic lattice. The model employed in this work is the same as that employed in ref 32, where a detailed description can be found. Only a brief account is given here.

2.1.1. Simple Cubic Lattice Model. In the simple cubic lattice model, a symmetric diblock copolymer chain of length N consists of the same number of A and B segments connected by bonds whose length is taken to be the lattice unit. Each segment occupies one lattice site, and each lattice site is occupied by at most one segment. In this work, a cubic simulation box of length L_b is employed.[43] Periodic boundary conditions (PBC) are imposed in all directions. We only consider a repulsive interaction energy $\epsilon_{AB} \geq 0$ between nonbonded nearest-neighbor A−B pairs separated by one lattice unit; we set $\epsilon_{AA} = \epsilon_{BB} = 0$. Interaction energies involving vacancies (unoccupied lattice sites) are also set to zero; these vacancies can therefore be viewed as neutral, good solvent molecules. We define our energy parameter as $\epsilon \equiv \epsilon_{AB}/k_BT$, where k_B is the Boltzmann's constant and T is the absolute temperature. A reduced temperature is defined as $T^* \equiv 1/\epsilon$.

2.1.2. Simulation Details. We perform Monte Carlo simulations in a variant of the expanded grand-canonical ensemble method proposed by Escobedo and de Pablo.[44] The chemical potential and temperature of the

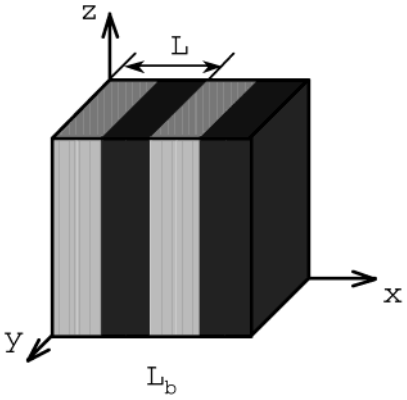

Figure 1. Schematics of the bulk lamellae in our simulations. Periodic boundary conditions are applied in all three directions of a cubic simulation box of length L_b. Two periods of lamellae with a period of $L = L_b/2$ form along the x axis.

system are specified prior to a simulation, and the density of the system (fraction of lattice sites occupied by copolymer segments) $\bar{\phi}_C$ is allowed to fluctuate. In addition to molecule displacements by reptation moves and local (kink−jump and crankshaft) moves, we make growing or shrinking attempts to gradually insert or remove chains from the system.[32] These moves are performed with two segments of type A and, simultaneously, two segments of type B. To facilitate transitions, a configurational bias scheme is introduced for these growing/shrinking moves.[32] As discussed later in section 3.1, some of our simulations are performed in the canonical (NVT) ensemble; only reptation and local moves are employed in those cases. Metropolis-like acceptance criteria are used in our simulations. One Monte Carlo step (MCS) consists of n_s reptation, local, and growing/shrinking (not employed in NVT simulations) trial moves, each of which occurs with the same probability; here $n_s \equiv \bar{\phi}_C V$, and $V = {L_b}^3$ is the volume of the system. After equilibrium is reached, $(4-15) \times 10^6$ MCS are used to calculate average properties.

We study symmetric diblock copolymers of chain lengths $N = 24$, 48, and 96. For each chain length, simulations are performed at three different temperatures ($\epsilon N = 10$, 20, and 40). The reduced chemical potential $\mu^* \equiv \ln(n_c/V) + \mu^E/(k_B T)$ is adjusted in each case such that $\bar{\phi}_C = 0.800$, where n_c is the total number of chains in the system, and μ^E is the excess chemical potential.[32] We also choose L_b in each case such that two periods of lamellae form along one of the coordinate axes of the box. We denote this axis as the x axis, as shown in Figure 1. These input parameters are listed in Table 2.

2.1.3. Alignment of Lamellar Profiles. Since PBC are applied in all directions, the lamellae move in the simulation box during the course of a simulation run, even along the x direction. Any variation along the x direction would therefore be smeared out for a long enough run, if the ensemble average is carried out in the fixed coordinates of the box. To avoid this, we need to "deduct" the motion of lamellae, i.e., to properly align each collected profile along the x direction.

In our previous work on lamellar structures,[32,45] we aligned the order parameter profile $\psi(x) \equiv \phi_A(x) - \phi_B(x)$ by setting its maximum at $x^* = 1$, where $\phi_A(x)$, for example, is the fraction of lattice sites occupied by A segments in the $y-z$ plane at given x, and x^* is the aligned coordinate. This is adequate for a *qualitative* description of the profile. However, due to the fluctuations of the system, when more than one period of lamellae is present along the x direction, such alignment breaks the periodicity of the profile and cannot be used for a *quantitative* study. We therefore use the method described below to align all the collected lamellar profiles along the x direction, including the order parameter profile $\psi(x)$, the segmental density profile for A blocks $\phi_A(x)$, the solvent density profile $\phi_S(x)$, the A-end distribution profile $E_A(x)$, and the A-joint segment (the A segments bonded to a B segment) distribution profile $J_A(x)$. The last two profiles are rescaled such that uniform distributions of A-end and A-joint segments in the system give $E_A(x) = 1$ and $J_A(x) = 1$, respectively.

Since we have two periods of lamellae along the x direction, each collected order parameter profile $\psi(x)$ has four roots x_i^0 ($i = 1$, ..., 4), where $\psi(x_i^0) = 0$. These roots are calculated by linear interpolation using the values of ψ at neighboring lattice positions x_k and x_{k+1} where $\psi(x_k)\psi(x_{k+1}) \le 0$. We then use $d \equiv (x_1^0 + x_2^0 + x_3^0 + x_4^0)/4$ to quantify the motion of lamellae along the x direction, which is shown in Figure 2. We align all the collected profiles by deducting the motion of the lamellae such that $\psi(x^* = 0) = 0$ and $(d\psi/dx^*)(x^* = 0) > 0$.

Because of the nature of the lattice model, each collected profile only has values at $x_k = 1$, ..., L_b. We refine the alignment by dividing one lattice spacing into 10 equal subintervals. In other words, d is significant

Table 2. List of Input Parameters and Some Results in Our Monte Carlo Simulations[a]

N	ϵN	μ^*	L_b	$\chi_\mu N$	s^2	$l/l_0 - 1$	r_g	r_{gb}	r_{AB}
24	10	41.0	24	29.39	0.715	0.1949	1.113	1.000	1.202
48	10	75.3	34	26.71	1.777	0.1893	1.114	0.999	1.208
96	10	145.3	48	23.57	3.366	0.2048	1.113	0.998	1.211
24	20	43.4	28	61.66	0.364	0.2073	1.181	1.011	1.309
48	20	77.9	40	57.97	0.891	0.1844	1.187	1.015	1.323
96	20	147.5	56	47.37	1.477	0.1922	1.185	1.015	1.324
24	40	46.9	28	179.8	0.257	0.0519	1.196	1.007	1.337
48	40	81.9	40	164.0	0.483	0.0119	1.200	1.012	1.347
96	40	151.3	56	134.4	0.788	−0.0122	1.196	1.012	1.346

[a] The resultant segmental density is $\bar{\phi}_C = 0.800$ for each simulation. l_0 denotes the equilibrium lamellar period predicted by the SCMF theory at corresponding $\chi_\mu N$. Refer to text for more details.

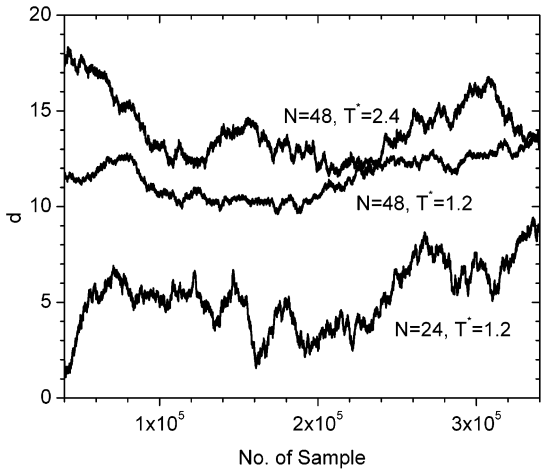

Figure 2. Motion of lamellae along the x axis (the direction perpendicular to the lamellar interfaces) during the course of a simulation run for given chain length N and reduced temperature T^*.

to one tenth when aligning the profiles. This is especially helpful when the A−B interfaces become sharp at low temperatures. In addition, due to the PBC, we have to assume that the motion of lamellae between two consecutively collected system configurations is small, so that we can track this motion and calculate x_i^0 ($i = 1$, ..., 4) without PBC; this is necessary to ensure $(d\psi/dx^*)$-$(x^* = 0) > 0$. Such an assumption is justified for our simulations. Finally, the ensemble-averaged, aligned profiles are averaged over their two periods before being compared with SCMF calculations. In the remainder of this paper, the superscript in x^* is dropped, and the lamellar period is denoted by $L = L_b/2$. For all the lamellar profiles shown here, $0 < x/L < 0.5$ corresponds to an A domain and $0.5 < x/L < 1$ corresponds to a B domain.

2.2. Self-Consistent Mean-Field Calculations. The SCMF theory for diblock copolymers has been discussed in detail in the literature.[46,47] We use n_c to denote the number of A−B diblock copolymer chains of length N in a system of volume V. The small-molecule solvent is denoted by S. We parametrize the segmental position on a chain by a variable $s \in [0, 1]$, where $s \le f_A$ corresponds to the A block, and $s \ge f_A$ corresponds to the B block; f_A is the volume fraction of A in the copolymer. The crux of an SCMF calculation is to solve the modified diffusion equation

$$\frac{\partial q_C}{\partial s} = \begin{cases} \frac{Na^2}{6}\nabla^2 q_C - \omega_A q_C & \text{if } s \le f_A \\ \frac{Na^2}{6}\nabla^2 q_C - \omega_B q_C & \text{if } s \ge f_A \end{cases} \quad (1)$$

where $q_C(\mathbf{r}, s)$ corresponds to the probability of finding a chain of length s that starts from $s = 0$ (A end) and ends at position $\mathbf{r}$, a is the Kuhn length of the chain (assumed to be the same for the two blocks), and $\omega_A(\mathbf{r})$, for example, is a mean field that interacts with the A blocks. By defining $t \equiv 1 - s$, a similar quantity $q_C^*(\mathbf{r}, t)$ can be defined, which corresponds to the probability of finding a chain of length t that starts from $t = 0$ (B end) and ends at position $\mathbf{r}$ and which satisfies

$$\frac{\partial q_C^*}{\partial t} = \begin{cases} \frac{Na^2}{6}\nabla^2 q_C^* - \omega_A q_C^* & \text{if } t \ge 1 - f_A \\ \frac{Na^2}{6}\nabla^2 q_C^* - \omega_B q_C^* & \text{if } t \le 1 - f_A \end{cases} \quad (2)$$

For the small-molecule solvent S, the modified diffusion equation becomes[47]

$$\frac{\partial q_S}{\partial s} = -\omega_S q_S \quad (3)$$

For given mean fields $\omega_A(\mathbf{r})$, $\omega_B(\mathbf{r})$, and $\omega_S(\mathbf{r})$, initial conditions $q_C(\mathbf{r}, s = 0) = 1$, $q_C^*(\mathbf{r}, t = 0) = 1$, and $q_S(\mathbf{r}, s = 0) = 1$ must be applied along with appropriate boundary conditions (e.g., periodic boundary conditions for bulk systems) to solve eqs 1−3, respectively. The densities $\phi_A(\mathbf{r})$, $\phi_B(\mathbf{r})$, and $\phi_S(\mathbf{r})$ can then be calculated from[48]

$$\phi_A = \frac{\bar{\phi}_C V}{z_C}\int_0^{f_A} q_C(\mathbf{r}, s) q_C^*(\mathbf{r}, 1 - s)\, ds \quad (4)$$

$$\phi_B = \frac{\bar{\phi}_C V}{z_C}\int_{f_A}^{1} q_C(\mathbf{r}, s) q_C^*(\mathbf{r}, 1 - s)\, ds \quad (5)$$

$$\phi_S = \frac{\bar{\phi}_S V}{z_S} q_S\left(\mathbf{r}, \frac{1}{N}\right) \quad (6)$$

where

$$z_C = \int q_C(\mathbf{r}, 1)\, d\mathbf{r} = \int q_C^*(\mathbf{r}, 1)\, d\mathbf{r} \quad (7)$$

$$z_S = \int q_S\left(\mathbf{r}, \frac{1}{N}\right) d\mathbf{r} \quad (8)$$

$\bar{\phi}_C$ and $\bar{\phi}_S$ are the average density of diblock copolymer segments and solvent molecules in the system, respectively. At any position $\mathbf{r}$, the mean fields are related to the densities by

$$\omega_A - \omega_S = \chi_{AB}N\phi_B + \chi_{AS}N(\phi_S - \phi_A) - \chi_{BS}N\phi_B \quad (9)$$

$$\omega_B - \omega_S = \chi_{AB}N\phi_A + \chi_{BS}N(\phi_S - \phi_B) - \chi_{AS}N\phi_A \quad (10)$$

where χ_{AB}, for example, is the Flory−Huggins interaction parameter between A and B segments. Note that $\bar{\phi}_C + \bar{\phi}_S = 1$ and that at any position $\mathbf{r}$

$$\phi_A + \phi_B + \phi_S = 1 \quad (11)$$

The above equations need to be solved self-consistently.

Having determined the densities and the mean fields, the free energy per chain of the system can be calculated as

$$f_c \equiv \frac{\Delta F^{\text{mixing}}}{n_c k_B T} = -\frac{1}{V}\int(\omega_A\phi_A + \omega_B\phi_B + \omega_S\phi_S - \chi_{AB}N\phi_A\phi_B - \chi_{AS}N\phi_A\phi_S - \chi_{BS}N\phi_B\phi_S)\, d\mathbf{r} - \bar{\phi}_C \ln\frac{z_C}{\bar{\phi}_C} - \bar{\phi}_S N \ln\frac{z_S}{\bar{\phi}_S} \quad (12)$$

where ΔF^{mixing} is the free energy of mixing. For an athermal solution where $\chi_{AB} = \chi_{AS} = \chi_{BS} = 0$, the free energy per chain becomes $f_{c,0} = \bar{\phi}_C \ln\bar{\phi}_C + \bar{\phi}_S N \ln\bar{\phi}_S$. The A-end and A-joint segment distributions defined above can be calculated as

$$E_A = \frac{NV}{z_C}\int_0^{1/N} q_C(\mathbf{r}, s) q_C^*(\mathbf{r}, 1 - s)\, ds \quad (13)$$

$$J_A = \frac{NV}{z_C}\int_{f_A-(1/N)}^{f_A} q_C(\mathbf{r}, s) q_C^*(\mathbf{r}, 1 - s)\, ds \quad (14)$$

We use the Douglas scheme[49] to solve the modified diffusion equations. This scheme is superior to the commonly used Crank−Nicolson scheme in that it provides higher accuracy in the space domain,[50] as shown later in Figure 9. Our solution to the SCMF equations is described in the Appendix. In this work, we set $f_A = 1/2$ and $\chi_{AS} = \chi_{BS} = 0$. The SCMF equations are solved for a one-dimensional unit cell that contains one period of lamellae and has volume $V = 1$.[51] By making the transformation $\mathbf{r} \to \mathbf{r}/R_{g,0}$, where the radius of gyration $R_{g,0} = a\sqrt{N/6}$ for a Gaussian chain of length N, the SCMF equations can be expressed in dimensionless form, where the only parameters left are the

average copolymer segmental density $\bar{\phi}_C$, the dimensionless unit cell length $l \equiv L/R_{g,0}$, the product of $\chi_{AB}N$, and the chain length N (this is not a parameter for the case of incompressible diblock copolymer melts). To compare with simulation results, values of these parameters are directly taken from simulations; note that, for a given ϵN, the value of $\chi_{AB}N$ is extracted in the various ways discussed in section 3.2. The subscript in χ_{AB} is dropped in the reminder of this paper.

2.3. Convolution Approximation. By virtue of its mean-field nature, the SCMF theory does not include fluctuation effects, one of which is the capillary-wave broadening of lamellar profiles along the x direction. For systems of large size in the other two (y and z) directions, this effect is significant and must be taken into account when comparing the profiles from mean-field theory with those from simulations or experiments.[42,52−57] We therefore use the convolution approximation to relate the broadened profile (denoted by the superscript "CONV") to its SCMF prediction (denoted by the superscript "SCMF"). This is achieved through expressions of the form

$$\phi_A^{CONV}(x;s^2) = \int_{-\infty}^{\infty} \phi_A^{SCMF}(x-u)P(u;s^2)\,du \quad (15)$$

where $P(u;s^2) \equiv \exp[-u^2/(2s^2)]/\sqrt{2\pi s^2}$ is the Gaussian distribution of the local A−B interfacial position and s^2 is the mean-square displacement of the interface. For single-interface systems (e.g.vapor−liquid interface or polymer blends), capillary-wave theory can provide certain predictions on the value of s^2.[56,58−60] For lamellae of diblock copolymers, however, a simple quantitative prediction for s^2 is not yet available.[42] We therefore follow ref 42; i.e., for a given $\phi_A^{SCMF}(x)$ and $\phi_B^{SCMF}(x)$ we adjust s^2 to obtain a least-squares fit between the broadened and the simulated segmental density profiles. A more detailed simulation study on the capillary-wave broadening of lamellar profiles is currently underway.[61]

3. Results and Discussion

3.1. Athermal Simulations for Estimation of $R_{g,0}$. As discussed above, $R_{g,0}$ provides the length scale for obtaining the dimensionless form of the SCMF equations in both cases of diblock copolymer melts and solutions. Because of the presence of solvent in our simulations, we calculate the mean-square radius of gyration of copolymer chains in a series of athermal simulations ($\epsilon = 0$) at different copolymer concentrations ($\bar{\phi}_C = 0.7$, 0.8, and 0.9), denoted by $R^2_{g,0}(\bar{\phi}_C)$, and then extrapolate the results linearly to obtain $R_{g,0} \equiv \sqrt{R_{g,0}{}^2(\bar{\phi}_C = 1)}$. These simulations are performed in a canonical ensemble with $L_b = 24$ (for $N = 24$) or 48 (for $N = 48$ and 96). The relative uncertainties in $R_{g,0}{}^2(\bar{\phi}_C)$ are $(1-5) \times 10^{-4}$ for all these simulations.

The results are shown in Figure 3a. A slight swelling of the chains is observed as $\bar{\phi}_C$ decreases; this is consistent with refs 16 and 62. The swelling is more noticeable for longer chains. Nevertheless, the increases of the radius of gyration in Figure 3a are at most about 3−5% of $R_{g,0}$. The scaling of $R_{g,0}{}^2(\bar{\phi}_C)$ with N obtained from our simulations is shown in Figure 3b for $\bar{\phi}_C = 0.8$ and 1.

3.2. Flory−Huggins χ Parameter. The χ parameter is introduced in the theory to characterize the energetic repulsion between A and B segments; in practice, however, χ is often viewed as a phenomenological parameter that corrects the simplified theoretical treatment of the energy and/or the entropy of a "realistic" (experimental or simulated) system. Therefore, when fitting experimental or simulation results using a theoretical formalism, the resultant value of χ depends on both the theory and the fitting process.

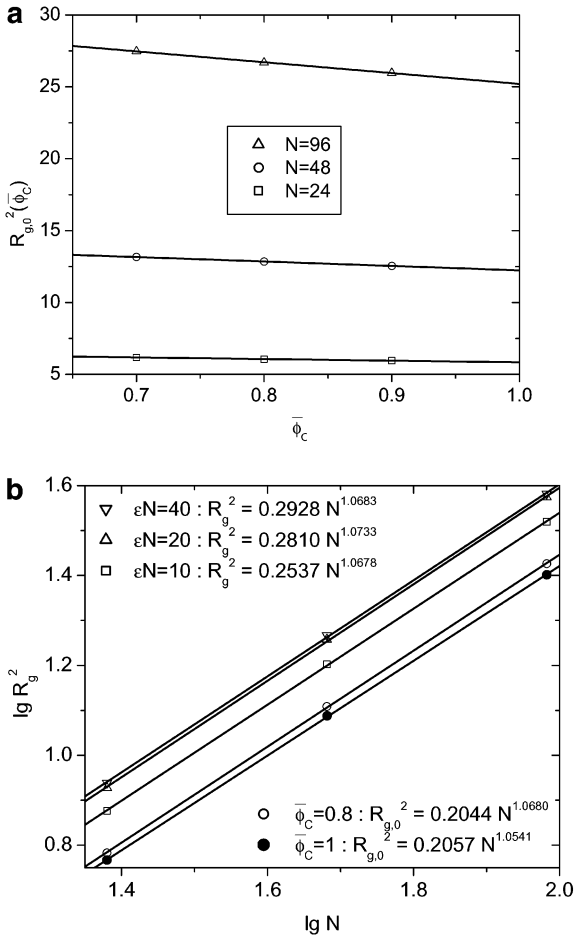

Figure 3. Mean-square radius of gyration of copolymer chains. (a) $R_{g,0}{}^2(\bar{\phi}_C)$ obtained in athermal simulations as a function of copolymer concentration $\bar{\phi}_C$. The solid lines are the linear, least-squares fit for each chain length N. (b) Scaling with N. $\bar{\phi}_C = 0.8$ for $\epsilon N = 10$, 20, and 40. The solid lines are the linear, least-squares fit with expressions displayed for corresponding conditions.

In previous simulations of diblock copolymers, the value of χ has been extracted from energy considerations. For lattice simulations, since ϵ is the actual "raw" parameter that characterizes the energetic repulsion between A and B segments, most simulation studies[14,16,18,20−22,25,28,41,42,63] have assumed that χ is directly related to ϵ by

$$\chi = \chi_A \equiv A\epsilon \quad (16)$$

where the proportionality constant A depends on the lattice type, but not on ϵ. For a χ_A based on the segmental energy E_s of the system, i.e.

$$\chi_A\bar{\phi}_A\bar{\phi}_B = E_s \equiv n_{AB}\epsilon/(V\bar{\phi}_C) \quad (17)$$

where n_{AB} is the total number of A−B contacts (nonbonded nearest-neighbor A−B pairs) in the system (it is assumed that each A−B contact results in the same energy ϵ), a mean-field, Flory-type formula of the form $n_{AB} = (z-2)\bar{\phi}_A\bar{\phi}_B V$ gives

$$\chi_A = \frac{z-2}{\bar{\phi}_C}\epsilon \tag{18}$$

where the coordination number is $z = 6$ for the simple cubic lattice employed in our simulations. In some other simulation studies,[20,28,31,64] the relation

$$\chi = \chi_{E,D} \equiv \frac{E_s}{\bar{\phi}_A\bar{\phi}_B} \tag{19}$$

has also been used, where E_s is obtained directly from simulations. Note that a disordered (homogeneous) phase is implied in both eqs 18 and 19, because $\bar{\phi}_A$ and ϕ_B are used to estimate χ. More appropriately, the following relation could be used

$$\chi = \chi_E \equiv \frac{E_s V}{\int \phi_A\phi_B \, d\mathbf{r}} \tag{20}$$

where E_s is again obtained directly from simulations. Here, eq 20 reduces to eq 19 for a disordered phase, and it accounts for the energy of an ordered phase in a more meaningful manner. Note that in the case of $\chi_{AS} = \chi_{BS} = 0$, $(N/V)\chi \int \phi_A\phi_B \, d\mathbf{r}$ is exactly the energy per chain $E_c \equiv E_s N$ in the SCMF theory. For a given N, the quantity $\int \phi_A\phi_B \, d\mathbf{r}$ in SCMF calculations depends on the value of χ; to obtain χ_E for a given ϵ, we adjust the value of χ_E such that the SCMF calculation gives the same energy as that obtained in simulations.

In contrast to all previous simulations of block copolymers, our simulations are performed at constant chemical potential. This provides us with the opportunity to make a direct connection between the SCMF theory and simulations based on the free energy of the system, which includes both entropic and energetic contributions. At a given $\bar{\phi}_C$, the difference in the reduced chemical potential of the copolymer in an ordered state and in the athermal solution, $\Delta\mu^*$, can be determined in SCMF calculations according to

$$\Delta\mu^* \equiv \mu^* - \mu_0^* = \left(f_c + \bar{\phi}_C\frac{df_c}{d\bar{\phi}_C}\right) - \left(f_{c,0} + \bar{\phi}_C\frac{df_{c,0}}{d\bar{\phi}_C}\right) \tag{21}$$

The values of μ^* in our expanded grand-canonical simulations are chosen to give $\bar{\phi}_C = 0.800$. Therefore, equating $\Delta\mu^*$ obtained from simulations with that obtained from eq 21 provides another way of extracting the χ parameter; we denote this value by χ_μ. In our SCMF calculations, $df_c/d\bar{\phi}_C$ is approximated by the central difference around the value of $\bar{\phi}_C$ obtained from simulations.

Figure 4 compares the values of χN obtained in the different ways outlined above. Large differences are found between χ_A and $\chi_{E,D}$, resulting from the assumption of constant n_{AB} used in eq 18. This assumption is in accordance with that used in eq 16, namely that A does not depend on ϵ; both of them are not appropriate for microphase-separated block copolymers. As seen from Figure 4, the segmental energy E_s obtained from simulations, which is directly proportional to $\chi_{E,D}$, exhibits a rather weak dependence on ϵ. This indicates that n_{AB} in simulations is nearly proportional to the reduced temperature T^*. Finally, if the SCMF theory agrees well with simulations, χ_E and χ_μ should be close to each other. However, in Figure 4 we see large differences between them, especially at low temperatures. This clearly reveals the complexity in the use of the Flory−Huggins χ parameter. In the reminder of this work we use $\chi_\mu N$ to make further comparisons between simulations and SCMF calculations. The values of $\chi_\mu N$ are listed in Table 2.

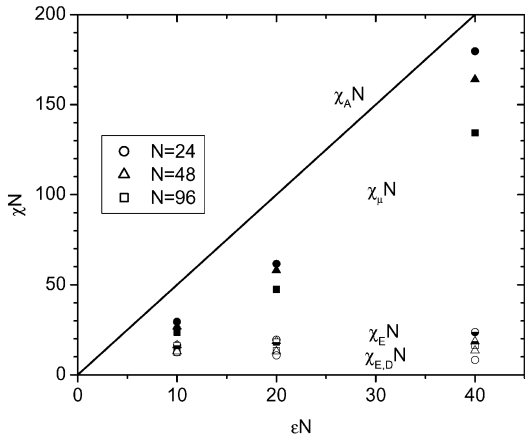

Figure 4. Comparison of the product of chain length N with the Flory−Huggins parameter χ extracted in different ways from simulations. The symbols of different shape correspond to different N, as shown in the legend. The solid line represents $\chi_A N$ from eq 18. For given ϵN and N, we have $\chi_A N > \chi_\mu N > \chi_E N > \chi_{E,D} N$. Refer to text for more details.

3.3. Segmental Density Profiles of One Block. As discussed in section 2.3, we use the convolution approximation and adjust the value of s^2 through a least-squares fit of simulated segmental density profiles; the resulting values of s^2 are listed in Table 2.

Parts a and b of Figure 5 show the density profiles of A blocks for $N = 24$ and 96, respectively, at different temperatures. We see that by taking the capillary-wave broadening into account good agreement is achieved between the simulated and calculated segmental density profiles; this is consistent with ref 42. Note, however, that $\phi_A^{CONV}(x)$ in the middle of the A domain is smaller than that obtained from simulations; the agreement improves for longer chains and weaker segregation. Also note that the local minimum of $\phi_A(x)$ in the middle of the A domain at stronger segregations is caused by the nonuniform distribution of solvent (vacancy) sites, which we shall discuss in section 3.4; in the case of $\bar{\phi}_C = 1$, $\phi_A(x)$ always has the maximum in the middle of the A domain.

3.4. Solvent Density Profiles. As mentioned earlier, the vacancies in our simulations can be viewed as neutral, good solvent molecules. They accumulate at lamellar interfaces to screen the repulsion between A and B segments, resulting in nonuniform solvent density profiles. Parts a and b of Figure 6 show the solvent density profiles at $\epsilon N = 10$ and 40, respectively. We characterize the maximum excess in the solvent density by $\Delta\phi_S^{max} \equiv \phi_S^{max} - \bar{\phi}_S = \phi_S^{max} - 0.2$, i.e., by the difference between the maximum and the average values of $\phi_S(x)$. The results for $\epsilon N = 20$ (not shown) exhibit the same qualitative features as those for $\epsilon N = 40$, with values of $\Delta\phi_S^{max}$ between those shown in Figure 6, parts a and b for the same N. We can see that the theoretical predictions are in qualitative agreement with simulations; $\Delta\phi_S^{max}$ occurs at the A−B interfaces, and it becomes smaller for larger N and for smaller ϵN. However, while the SCMF predictions (at $\chi_\mu N$) overestimate the variation of $\phi_S(x)$, the least-squares fit of

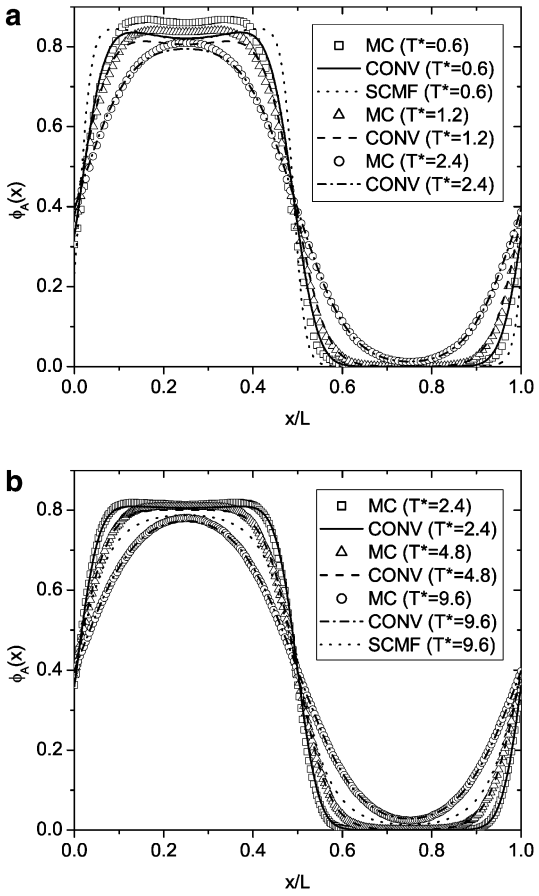

Figure 5. Segmental density profiles of A blocks $\phi_A(x)$ at (a) $N = 24$ and (b) $N = 96$. The values of $\chi_\mu N$ and s^2 used in the SCMF calculations and the convolution approximation are listed in Table 2.

segmental density profiles underestimates it by about 50% in all cases.

In our SCMF calculations, the largest $\Delta\phi_S^{max}$ is about 0.288 (for the case of $N = 24$ and $\chi_\mu N = 179.8$, shown in Figure 6b); the small variation of $\phi_S(x)$ ($\Delta\phi_S^{max} < 0.04$) obtained by Whitmore and Noolandi is due to their longer chain lengths ($100 \le N \le 2000$)[65]. Actually, from eqs 3, 6, and 8, we obtain for large N and small $\omega_S(\mathbf{r})$ (small χN)

$$\phi_S - \bar{\phi}_S \approx -\frac{\omega_S}{N}\bar{\phi}_S \qquad (22)$$

Other interesting features of the solvent density profiles are the local maxima in the middle of the A and B domains, which appear in our simulations for the $\epsilon N = 20$ and 40 cases, but not for the $\epsilon N = 10$ case. While the SCMF calculations (at $\chi_\mu N$) exhibit local maxima in all cases, most of the discrepancies for the $\epsilon N = 10$ case are resolved by the convolution approximation. As shown in Table 2, for the $\epsilon N = 10$ and 20 cases, the lamellar period l specified in our simulations is about 20% larger than l_0 (the dimensionless equilibrium lamellar period that minimizes the free energy per chain) predicted by the SCMF theory at corresponding $\chi_\mu N$; lamellae are therefore stretched in these SCMF calculations. As pointed out by Whitmore and Noolandi, this stretching of lamellae could give rise to the local maxima of $\phi_S(x)$ in SCMF calculations.[65] In contrast to their finding that local maxima do not occur at l_0,[65] we do observe local maxima in our SCMF calculations at

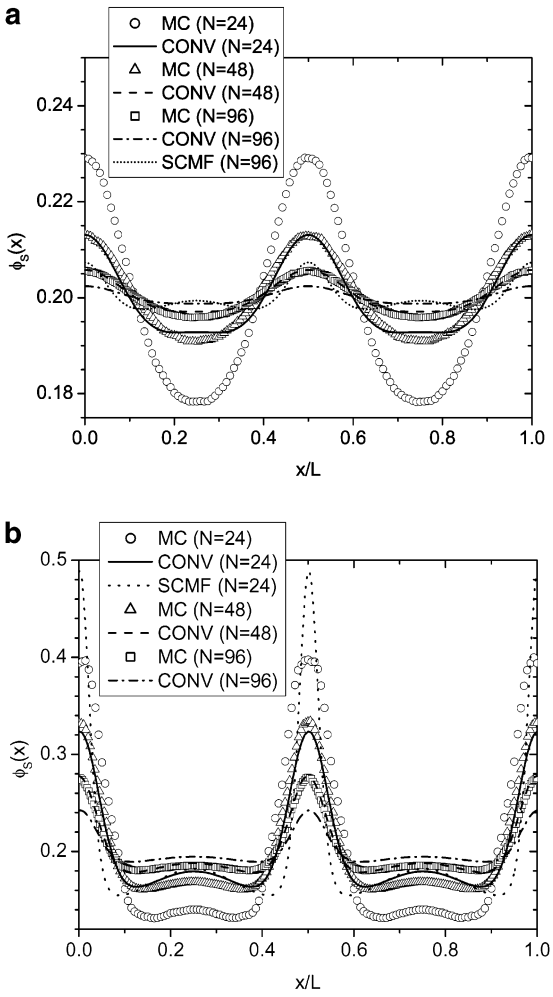

Figure 6. Solvent density profiles $\phi_S(x)$ at (a) $\epsilon N = 10$ and (b) $\epsilon N = 40$. The values of $\chi_\mu N$ and s^2 used in the SCMF calculations and the convolution approximation are listed in Table 2.

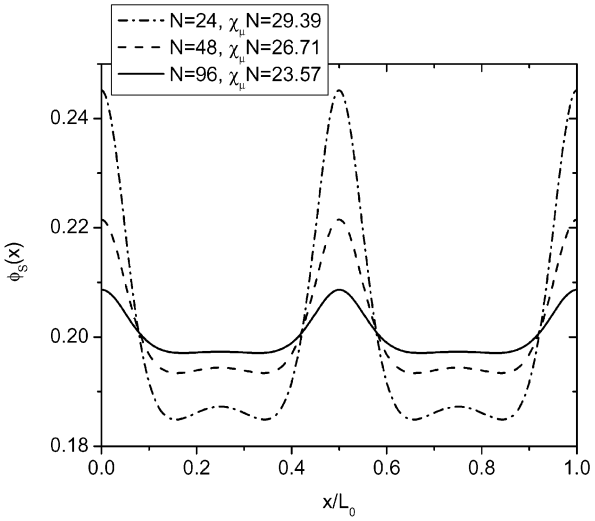

Figure 7. Solvent density profiles $\phi_S(x)$ at equilibrium lamellar period L_0 predicted by the SCMF theory.

l_0 for all values of $\chi_\mu N$ listed in Table 2; this is shown in Figure 7 for the cases corresponding to $\epsilon N = 10$. These local maxima become more pronounced for shorter chains and larger χN; only for longer chains and smaller χN do they vanish.

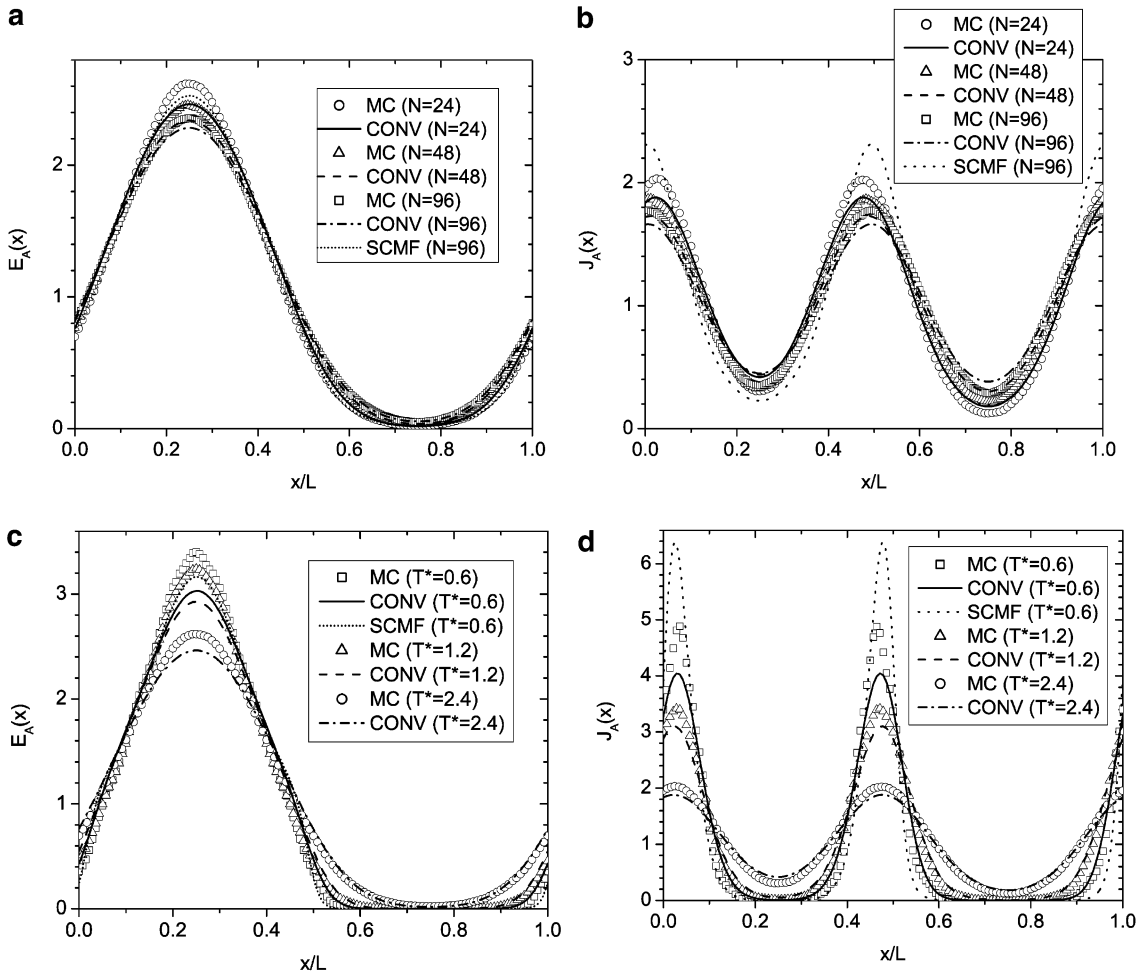

Figure 8. A-end distribution $E_A(x)$ and A-joint segment distribution $J_A(x)$. Uniform distributions of A-ends and A-joint segments in the system would give $E_A(x) = 1$ and $J_A(x) = 1$, respectively. Parts a and b present results for $\epsilon N = 10$; parts c and d present results for chain length $N = 24$. The values of $\chi_\mu N$ and s^2 used in the SCMF calculations and the convolution approximation are listed in Table 2.

3.5. Chain End and Joint Segment Distributions. Parts a and b of Figure 8 show the A-end and A-joint segment distributions $E_A(x)$ and $J_A(x)$, respectively, at $\epsilon N = 10$. (Recall that uniform distributions of A-ends and A-joint segments give $E_A(x) = 1$ and $J_A(x) = 1$, respectively.) Both simulations and theoretical calculations show slightly broader distributions of $E_A(x)$ and $J_A(x)$ for larger N. Parts c and d of Figure 8 show $E_A(x)$ and $J_A(x)$, respectively, for $N = 24$. As expected, chain ends and joint segments are more localized at lower temperatures. However, the distribution of chain ends is much less sensitive to temperature than that of joint segments. This is because the distribution of chain ends is mainly entropy-dominated, while that of joint segments is mainly energy-dominated. Therefore, even at the lowest temperature $T^* = 0.6$ ($N = 24$ and $\chi_\mu N = 179.8$), where the system is considered to be in the strong segregation regime according to the square-wavelike $\phi_A(x)$ shown in Figure 5a, we still have a broad distribution of A-ends within the A domain, while the A-joint segments are highly localized at the A−B interfaces.

In all cases, the least-squares fit of the segmental density profiles gives broader distributions for both $E_A(x)$ and $J_A(x)$ than those obtained from simulations. As expected, the shorter the chain length and the stronger the segregation, the larger the discrepancy. As shown above, the same trends are observed on both $\phi_A(x)$ and $\phi_S(x)$.

3.6. On the Equilibrium Lamellar Period. From our bulk simulation data presented in ref 32, which were obtained from extensive simulations for symmetric diblock copolymers of $N = 24$, we estimate the equilibrium lamellar period to be $L_0 = 12 \pm 0.1$ (in units of lattice spacing) at $T^* = 2.4$ and $\mu^* = 41$; this gives $l_0 \equiv L_0/R_{g,0} = 4.96 \pm 0.04$. However, our SCMF calculations for $N = 24$ at the corresponding $\chi_\mu N$ and the same $\bar{\phi}_C = 0.800$ give $l_0 = 4.154$, about 16% smaller than that obtained from simulations. Since chain swelling at this high $\bar{\phi}_C$ is rather small (about 2% of $R_{g,0}$), it cannot explain this discrepancy. Because of the excessive computational demands,[32,36] we have not estimated L_0 for other chain lengths and temperatures from simulations and therefore cannot make further comparisons with the SCMF theory at this point.

3.7. On the Scaling with ϵN. Fried and Binder proposed that ϵN is an approximate scaling variable for static properties of symmetric diblock copolymers; the relaxation time for the slowest fluctuation modes of the system, N/S^* (where S^* denotes the maximum value of the spherically averaged collective structure factor), $q^*R_g(\bar{\phi}_C)$ (where q^* locates S^*), $r_g \equiv R_g(\bar{\phi}_C)/R_{g,0}(\bar{\phi}_C)$, $r_{AB} \equiv R_{AB}/R_{AB,0}$ (where R_{AB} denotes the distance between the center-of-mass of A and B blocks of the same chain,

and the subscript 0 denotes the athermal condition), and $r_i \equiv R_i/R_{i,0}$ (where R_i denotes the copolymer principal radii, $i = 1, 2, 3$), all approximately scale with ϵN.[14,15] The scalings of r_g and r_{AB} were confirmed in simulations by Weyersberg and Vilgis, where they also reported a scaling of $d_{ee} \equiv D_{ee}(\bar{\phi}_C)/D_{ee,0}(\bar{\phi}_C)$ (where D_{ee} denotes the chain end-to-end distance) with ϵN, and an almost constant $r_{gb} \equiv R_{gb}(\bar{\phi}_C)/R_{gb,0}(\bar{\phi}_C) \approx 1$ (where R_{gb} denotes the block radius of gyration).[16] They also showed that r_g is almost independent of $\bar{\phi}_C$ for $0.6 \leq \bar{\phi}_C \leq 1$.[16] Hoffmann and co-workers reported that S_0^*/S^*, $q^*R_{g,0}(\bar{\phi}_C)$, the ratio of the average domain size estimated from box-counting to $R_{g,0}(\bar{\phi}_C)$, r_g, r_{AB}, and r_{gb}, all scale with ϵN.[29]

In earlier simulations the quantities of interest were calculated for different N and at different T^*, but with a simulation box having two or three equal sides of arbitrary length.[14−16,29] For ordered lamellar phases, the mismatch between the periodic boundary conditions (PBC) and L_0 (which varies with both N and T^*) influences significantly the results of simulations and, in some cases, gives rise to large deviations of L from L_0. The large scatter of earlier scaling simulation data within and below the range of the ODT, as compared to their results for the disordered phase,[14−16,29] could be partly due to such mismatch. References 17 and 26 have clearly demonstrated the influence of different specified lamellar period L on various quantities of interest. Better scaling data were obtained by Kremer and co-workers using constant-pressure molecular dynamics, where L was automatically adjusted to L_0 during the simulation.[27,30]

To alleviate some of the problems of constant-volume simulations, in this work we carefully choose the box sizes according to the estimated L_0 for $N = 24$ at $T^* = 2.4$. Note, however, that the mismatch between the PBC and L_0 cannot be completely eliminated because of the lattice model. Nevertheless, we expect the influence of the mismatch to be small in our simulations. Our results for r_g and r_{AB}, listed in Table 2, exhibit good scaling with ϵN in the ordered lamellar phase, even in the strong segregation regime at $\epsilon N = 40$. We also see from Table 2 that the dependence of r_{gb} on ϵN is fairly weak, at least for the ordered phase. Differences in profiles for various N at the same ϵN (see Figure 6, as well as Figure 8, parts a and b), however, suggest that for chain lengths considered here ϵN may not be an ideal scaling variable for quantities related to the collective structure factor of the ordered phase.

The good scaling of r_g with ϵN, even in the strong segregation regime, indicates that $R_g(N) \propto N^{1/2}$ (at constant ϵN) for highly concentrated solutions or melts, regardless of the degree of segregation. This is confirmed by our results shown in Figure 3b. It has been shown that, due to the repulsion between A and B segments, chain-stretching occurs even at temperatures well above the ODT; the copolymer chain conformation is therefore not Gaussian, except under athermal conditions.[13−18,21,23,25−31,33,35,36] Therefore, the $R_g(N) \propto N^{1/2}$ relation is not equivalent to the Gaussian chain conformation; the $R_{AB}(N)/R_g(N) = \sqrt{2}$ relation proposed by Fried and Binder[14] provides a better characterization of Gaussian behavior for symmetric diblock copolymers.

4. Conclusions

We have quantitatively examined the predictions of a self-consistent mean-field (SCMF) formalism by comparing them with results of Monte Carlo simulations for bulk lamellar structures of symmetric diblock copolymers A−B in concentrated solutions of a neutral, good solvent. A convolution approximation is used to take into account the capillary-wave broadening of lamellar profiles, which is absent in the SCMF theory. In dimensionless form, the SCMF equations for the system of interest have four input parameters: the average copolymer segmental density $\bar{\phi}_C$, the dimensionless unit cell length l, the chain length N (this is not a parameter for the case of incompressible diblock copolymer melts), and the product χN (where χ is the Flory−Huggins parameter for the repulsion between A and B segments). In this work, values of these parameters are directly taken from simulations, except that the value of χ is extracted from simulations at a given ϵ (the actual parameter used in simulations to characterize the A−B repulsion) in different ways, namely from the energies or chemical potentials of the copolymers; these values are denoted by χ_E and χ_μ, respectively.

Large differences are observed between the values of χ_E and χ_μ, particularly at low temperatures. The product of $\chi_\mu N$, rather than $\chi_E N$, provides a suitable measure of the degree of segregation of symmetric diblock copolymers. On the basis of the segmental density profiles predicted by the SCMF theory at $\chi_\mu N$, we adjust the mean-square displacement of the local A−B interfaces (a parameter in the convolution approximation) to achieve a least-squares fit of simulated segmental density profiles. We then compare the solvent density profile, as well as the chain end and joint segment distributions, without further adjustable parameters. While the theoretical predictions are in qualitative agreement with simulation results, we see that the shorter the chain length and the lower the temperature, the larger the discrepancy between these two. We find that theoretical predictions underestimate by about 50% the variation of solvent density profiles caused by the segregation of the neutral solvent at A−B interfaces. This could be of importance in the context of recent applications of the SCMF theory to the study of solvent effects in block copolymer solutions.[47,66,67] The SCMF theory also seems to underestimate the equilibrium lamellar period.

Our simulations show good scaling of chain dimensions with the interaction parameter ϵN, even in the strong segregation regime; this implies that the radius of gyration of diblock copolymer chains $R_g(N)$ is proportional to $N^{1/2}$ (at constant ϵN) for highly concentrated solutions or melts, regardless of the degree of segregation.

Acknowledgment. The authors are grateful to Dr. Adnan Rebei and Dr. Marcus Müller for helpful discussions. Financial support for this work was provided by the Semiconductor Research Corp. through Contract No.99-LP-452 and by the NSF,CTS-0210588, and EEC-0085560.

5. Appendix

We discretize the space domain into m nodes, denoted by $\mathbf{r}_i$ ($i = 1, ..., m$). We represent the values of any variable $p(\mathbf{r})$ at these nodes by a vector $\mathbf{p} \equiv [p(\mathbf{r}_1), p(\mathbf{r}_2), ..., p(\mathbf{r}_m)]^T$. The SCMF equations can then be rewritten into a set of nonlinear equations $(\mathbf{F}_1[\omega_A, \omega_B], \mathbf{F}_2[\omega_A, \omega_B])^T$

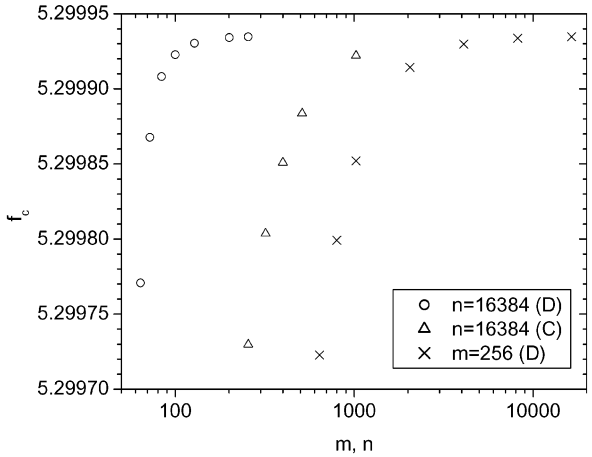

Figure 9. Accuracy in the free energy per chain f_c for incompressible symmetric diblock copolymer melts ($\bar{\phi}_C = 1$) at $\chi N = 40$ and the dimensionless unit cell length $l = 4.773$. m and n are the number of subintervals in the space domain and the time domain (the s domain), respectively. In the legend, C denotes the Crank−Nicolson scheme, and D denotes the Douglas scheme.

$= 0$ with ω_A and ω_B being the independent variables, i.e.at each node

$$F_1 = \omega_A - \omega_B - \chi_{AB}N(\phi_B - \phi_A) - (\chi_{AS} - \chi_{BS})N(1 - \phi_C) \quad (23)$$

$$\phi_C = \phi_A + \phi_B \quad (24)$$

$$F_2 = \phi_C - 1 + \frac{\bar{\phi}_S V \exp(-\omega_S/N)}{\int \exp(-\omega_S/N)\, d\mathbf{r}} \quad (25)$$

$$\omega_S = \frac{\omega_A + \omega_B - \chi_{AB}N\phi_C}{2} + N(\chi_{AS}\phi_A + \chi_{BS}\phi_B) - \frac{(\chi_{AS} + \chi_{BS})N(1 - \phi_C)}{2} \quad (26)$$

In the case where ϕ_C is given, e.g., incompressible diblock copolymer melts[46] or specified density profile of diblock copolymers near hard walls,[68] eqs 24−26 are replaced by

$$F_2 = \phi_C - \phi_A - \phi_B \quad (27)$$

ϕ_A and ϕ_B in the above nonlinear equations are calculated from eqs 1, 2, 4, 5, and 7. We solve this set of nonlinear equations by a quasi-Newton method.[69] Note that only $2m - 1$ out of the $2m$ variables ω_A and ω_B need to be solved; i.e., we have only $2m - 1$ unknowns. This is seen from the fact that if a set of ω_A^* and ω_B^* is the solution, then the set of $\omega_A^* + c$ and $\omega_B^* + c$ is also the solution with c being an arbitrary constant (i.e., they result in the same densities and the same free energy). Therefore, an arbitrary value must be assigned to one of the $2m$ variables, e.g., $\omega_A(\mathbf{r}_1)$.

We employ the Douglas scheme,[50] a finite difference scheme having a second-order accuracy in the time domain (in our case the s domain) and a fourth-order accuracy in the space domain, to solve the modified diffusion equations. The space domain and the time domain are discretized into m and n equal subintervals, respectively. Figure 9 demonstrates the accuracy of f_c in our calculations for incompressible symmetric diblock copolymer melts ($\phi_C = 1$ at any position $\mathbf{r}$) at $\chi N = 40$ and $l = l_0 = 4.773$. The Douglas scheme with $m \geq 200$ and $n \geq 10^4$ ($m \geq 80$ and $n \geq 2000$) gives an accuracy of $\pm 10^{-5}$ ($\pm 10^{-4}$) in f_c at $\chi N = 40$. As χN increases, the variation of the densities and the mean fields in the system also increases, and larger m and n are required to reach a target accuracy. In most of our theoretical calculations, we use $n = 3840$, 7680, and 15360 for $\epsilon N = 10$, 20, and 40, respectively, and $240 \leq m \leq 400$ (depending on the size of the simulation box); we estimate that our accuracy in f_c is between $\pm 10^{-7}$ and $\pm 10^{-4}$ for these calculations. The only exception is that $m = 2240$ (or 2400) and $n = 7680$ are used when we perform calculations at $\chi_\mu N$ corresponding to $\epsilon N = 40$, which gives an accuracy of $\pm 10^{-2}$ in f_c.

References and Notes

(1) Bates, F. S.; Fredrickson, G. H. *Annu. Rev. Phys. Chem.* **1990**, *41*, 525.
(2) Helfand, E.; *Macromolecules*, **1975**, *8*, 552.
(3) Helfand, E.; Wasserman, Z. R. *Macromolecules* **1976**, *9*, 879.
(4) Helfand, E.; Wasserman, Z. R. *Macromolecules* **1978**, *11*, 960.
(5) Helfand, E.; Wasserman, Z. R. *Macromolecules* **1980**, *13*, 994.
(6) Leibler, L.; *Macromolecules* **1980**, *13*, 1602.
(7) Thompson, R. B.; Ginzburg, V. V.; Matsen, M. W.; Balazs, A. C. *Science* **2001**, *292* (5526), 2469.
(8) Thompson, R. B.; Ginzburg, V. V.; Matsen, M. W.; Balazs, A. C. *Macromolecules* **2002**, *35*, 1060.
(9) Lee, J. Y.; Thompson, R. B.; Jasnow, D.; Balazs, A. C. *Macromolecules* **2002**, *35*, 4855.
(10) Whitmore, M. D.; Vavasour, J. D. *Acta Polym.* **1995**, *46*, 341.
(11) Matsen, M. W.; Bates, F. S. *Macromolecules* **1996**, *29*, 1091.
(12) Chakrabarti, A.; Toral, R.; Gunton, *J. D. Phys. Rev. Lett.* **1989**, *63*, 2661.
(13) Minchau, B.; Dunweg, B.; Binder, K. *Polym. Commun.* **1990**, *31*, 348.
(14) Fried, H.; Binder, K. *J. Chem. Phys.* **1991**, *94*, 8349.
(15) Fried, H.; Binder, K. *Europhys. Lett.* **1991**, *16* (3), 237.
(16) Weyersberg, A.; Vilgis, T. A. *Phys. Rev. E* **1993**, *48*, 377.
(17) Balaji, R.; Wang, Y.; Foster, M. D.; Mattice, W. L. *Comput. Polym. Sci.* **1993**, *3* (1&2), 15.
(18) Molina, L. A.; Rodriguez, A. L.; Freire, J. J. *Macromolecules* **1994**, *27*, 1160.
(19) Haliloglu, T.; Balaji, R.; Mattice, W. L. *Macromolecules* **1994**, *27*, 1473.
(20) Yang, Y.; Lu, J.; Yan, D.; Ding, J. *Macromol. Theory Simul.* **1994**, *3*, 731.
(21) Larson, R. G.; *Mol. Simul.* **1994**, *13*, 321.
(22) Larson, R. G.; *Macromolecules* **1994**, *27*, 4198.
(23) Molina, L. A.; Freire, J. J. *Macromolecules* **1995**, *28*, 2705.
(24) Ko, M. B.; Mattice, W. L. *Macromolecules* **1995**, *28*, 6871.
(25) Pan, X.; Shaffer, J. S. *Macromolecules* **1996**, *29*, 4453.
(26) Dotera, T.; Hatano, A. *J. Chem. Phys.* **1996**, *105*, 8413.
(27) Grest, G. S.; Lacasse, M.-D.; Kremer, K.; Gupta, A. M. *J. Chem. Phys.* **1996**, *105*, 10583.
(28) Pakula, T.; Karatasos, K.; Anastasiadis, S. H.; Fytas, G. *Macromolecules* **1997**, *30*, 8463.
(29) Hoffmann, A.; Sommer, J.-U.; Blumen, A. *J. Chem. Phys.* **1997**, *106*, 6709.
(30) Murat, M.; Grest, G. S.; Kremer, K. *Macromolecules* **1999**, *32*, 595.
(31) Jo, W. H.; Jang, S. S. *J. Chem. Phys.* **1999**, *111*, 1712.
(32) Wang, Q.; Yan, Q.; Nealey, P. F.; de Pablo, J. J. *J. Chem. Phys.* **2000**, *112*, 450.
(33) Binder, K.; Fried, H. *Macromolecules* **1993**, *26*, 6878.
(34) Micka, U.; Binder, K. *Macromol. Theory Simul.* **1995**, *4*, 419.
(35) Hoffmann, A.; Sommer, J.-U.; Blumen, A. *J. Chem. Phys.* **1997**, *107*, 7559.
(36) Wang, Q.; Nealey, P. F.; de Pablo, J. J. *Macromolecules* **2001**, *34*, 3458.
(37) Carmesin, I.; Kremer, K. *Macromolecules* **1988**, *21*, 2819. Larson, R. G.; *J. Chem. Phys.* **1988**, *89*, 1642.
(38) Binder, K.; Muller, M. *Curr. Opin. Colloid Interface Sci.* **2000**, *5*, 315.
(39) Fredrickson, G. H.; Helfand, E. *J. Chem. Phys.* **1987**, *87*, 697.
(40) Barrat, J.-L.; Fredrickson, G. H. *J. Chem. Phys.* **1991**, *95*, 1281.

(41) Geisinger, T.; Muller, M.; Binder, K. *J. Chem. Phys.* **1999**, *111*, 5241.
(42) Geisinger, T.; Muller, M.; Binder, K. *J. Chem. Phys.* **1999**, *111*, 5251.
(43) This is different from ref 32 where rectangular boxes with three unequal sides were used to provide as many "options" for the lamellar period as possible; here a cubic box is the most suitable for our purpose of specifying the lamellar period *L*.
(44) Escobedo, F. A.; de Pablo, J. J. *J. Chem. Phys.* **1996**, *105*, 4391.
(45) Wang, Q.; Yan, Q.; Nealey, P. F.; de Pablo, J. J. *Macromolecules* **2000**, *33*, 4512.
(46) Matsen, M. W.; Schick, M. *Phys. Rev. Lett.* **1994**, *72*, 2660.
(47) Huang, C.-I; Lodge, T. P. *Macromolecules* **1998**, *31*, 3556.
(48) There is a typographical mistake in eq 5 of ref 47.
(49) Douglas, J.; Jr. *J. Math. Phys.* **1956**, *35*, 145.
(50) Chapter 2.4 in Mitchell, A. R.; Griffiths, D. F. *The Finite Difference Method in Partial Differential Equations*; Wiley: Chichester, England, and New York, 1980.
(51) Different values of *V* actually result in the same densities and the same free energy.
(52) Shull, K. R.; Mayes, A. M.; Russell, T. P. *Macromolecules* **1993**, *26*, 3929.
(53) Semenov, A. N.; *Macromolecules* **1993**, *26*, 6617.
(54) Semenov, A. N.; *Macromolecules* **1994**, *27*, 2732.
(55) Kerle, T.; Klein, J.; Binder, K. *Phys. Rev. Lett.* **1996**, *77*, 1318.
(56) Sferrazza, M.; Xiao, C.; Jones, R. A. L.; Bucknall, D. G.; Webster, J.; Penfold, *J. Phys. Rev. Lett.* **1997**, *78*, 3693.
(57) Koneripalli, N.; Levicky, R.; Bates, F. S.; Matsen, M. W.; Satija, S. K.; Ankner, J.; Kaiser, H. *Macromolecules* **1998**, *31*, 3498.
(58) Buff, F. P.; Lovett, R. A.; Stillinger, F. H. Jr. *Phys. Rev. Lett.* **1965**, *15*, 621.
(59) Rowlinson, J. S.; Widom, B. *Molecular Theory of Capillarity*; Oxford University Press: Oxford, U.K., 1982.
(60) Binder, K.; Muller, M.; Schmid, F.; Werner, A. *Adv. Colloid Interface Sci.* **2001**, *94*, 237.
(61) Wang, Q.; Muller, M.; de Pablo, J. J. Manuscript in preparation.
(62) Olaj, O. F.; Petrik, T.; Zifferer, G. *Macromol. Theory Simul.* **1997**, *6*, 1277.
(63) Huh, J.; Ginzburg, V. V.; Balazs, A. C. *Macromolecules* **2000**, *33*, 8085.
(64) An extra factor of 2 is added to the denominator of eq 9 in ref 31.
(65) Whitmore, M. D.; Noolandi, J. *J. Chem. Phys.* **1990**, *93*, 2946.
(66) Lodge, T. P.; Hamersky, M. W.; Hanley, K. J.; Huang, C.-I *Macromolecules* **1997**, *30*, 6139.
(67) Hanley, K. J.; Lodge, T. P.; Huang, C.-I *Macromolecules* **2000**, *33*, 5918.
(68) Matsen, M. W. *J. Chem. Phys.* **1997**, *106*, 7781.
(69) Broyden, C. G. *Math. Comput.* **1965**, *19*, 577.

MA0203905